Thesis for Master Degree

Thermodynamic Stability, Spectroscopic Identification, and Gas Storage Capacity of N_2O and N_2 Mixtures Gas Hydrates

아산화질소-질소 혼합가스 하이드레이트의 상평형, 분광학적 분석 및 가스저장 성능에 관한 연구

Advisor: Prof. Yoon, Ji-Ho

February 2017

Department of Convergence Study on the Ocean Science and Technology
School of Ocean Science and Technology
Korea Maritime and Ocean University

Yang, Youjeong

Thesis for Master Degree

Thermodynamic Stability, Spectroscopic Identification, and Gas Storage Capacity of N_2O and N_2 Mixtures Gas Hydrates

아산화질소-질소 혼합가스 하이드레이트의 상평형, 분광학적 분석 및 가스저장 성능에 관한 연구

Advisor: Prof. Yoon, Ji-Ho

February 2017

Department of Convergence Study on the Ocean Science and Technology
School of Ocean Science and Technology
Korea Maritime and Ocean University

Yang, Youjeong

Approved by the Committee of the Ocean Science and Technology School of Korea Maritime and Ocean University in Fulfillment of the Requirements for the Degree of Master´ s in Engineering

Dissertation Committee :

Prof. Kim, Dongseon, Chair _____

Prof. Yoon, Ji-Ho, Advisor _____

Prof. Yoo, Kyoungkeun, Advisor _____

February 2017

Department of Convergence Study on the Ocean Science and Technology

Ocean Science and Technology School

Korea Maritime and Ocean University

Table of Contents

List of Tables

List of Figures

아산화질소-질소 혼합가스 하이드레이트의 상평형, 분광학적 분석 및 가스저장 성능에 관한 연구

양 유 정

해양과학기술융합학과

한국해양대학교 해양과학기술전문대학원

초 록

아산화질소/질소(N_2O/N_2) (100/0, 80/20, 60/40, 40/60, 20/80) 혼합가스 하이드레이트를 분광학적으로 구조적 분석과 객체 분자의 거동을 측정하였다. Powder X-ray diffraction (XRD) 분석 결과, 모든 혼합비의 아산화질소/질소 하이드레이트는 SI 구조를 형성하였다. Raman spectroscopy를 통하여 아산화질소/질소 혼합가스 하이드레이트에 포집된 아산화질소 분자의 객체 포집 거동과 동공 포집률 변이를 측정하였다. 순수 아산화질소 가스 하이드레이트의 경우, υ_1과 υ_3 범위에서 2개의 라만 밴드가 나타나는데 이것은 아산화질소 분자가 S1 구조의 작은 동공과 큰 동공에 포집되었음을 의미한다. 아산화질소/질소(20/80) 혼합가스 하이드레이트의 경우, 1개의 라만 밴드가 측정된 것으로 보아 아산화질소가 S1구조의 작은 동공에만 포집되었음을 알 수 있었다. 반면, 아산화질소-테트라하이드로퓨란(THF) 5.56 mol% SII 하이드레이트의 경우 υ_1과 υ_3 범위에서 관측된 1개의 라만 밴드는 아산화질소 분자가 SII 구조의 작은 동공에 포집된 것을 의미한다. 라만 결과를 이용하여 아산화질소/질소 혼합가스 SI 하이드레이

트의 작은 동공과 큰 동공의 포집률을 추정하여 나타내었다. 아산화질소/질소 혼합가스 하이드레이트의 상평형은 274-286 K 온도 범위와 최대 8.4 MPa 압력 범위에서 측정되었다. 순수 아산화질소 하이드레이트와 아산화질소/질소(40/60) 혼합 하이드레이트의 온도변이에 따른 라만측정을 수행했고 아산화질소와 질소의 자기보존 현상을 발견하였다. 마지막으로, 아산화질소/질소 혼합가스 하이드레이트에 대한 가스저장량을 제시하였다.

Key Words : Nitrous oxide 아산화질소, Clathrate hyrdrate 포접 수화물, Phase equilibrium 상평형, Spectroscopic identification 분광학적 분석, Cage occupancy 동공 포집율.

Chapter 1. Introduction

1.1. Background

1.1.1 Nitrous Oxide

Nitrous oxide (N_2O) is one of the principal substances depleting the ozone layer (Ravishankara et al, 2009, 2012). It is defined as one of the main greenhouse gases (GHGs) and has a significant global warming potential (GWP)—one metric ton of N_2O is equal to 310 metric tons of carbon dioxide (CO_2) as shown in Table 1 (IPCC, 2007). Since 1750, the emission quantity of N_2O in the atmosphere has increased by over 15 percent and is expected to continuously increase due to its recent use in various fields as an anesthetic substance, such as in operations, culinary use, rocketry, and internal engine combustion (Metz et al., 2007). N_2O gas is released from various natural and anthropogenic sources, with the main natural N_2O emission sources being biological processes in soil and the oceans. Even though the chemical industry is a minor source of emission, it is a significant human-produced source. When several chemical substances such as nitic acid and adipic acid, commonly created by the process of catalytic oxidation of ammonia, are manufactured, N_2O gas is undesirably generated as a by-product (U.S. EPA, 2010). Anthropogenic activities largely comprise: 1) the agricultural field; 2) fuel combustion; 3) the energy and chemical industries; and 4) the waste management of nitrogen-based organic substances (Table 2). Although agricultural activities are the largest source of human-made N_2O, owing to the limitation of current technologies the industrial source is the most appropriate point to trap and reduce such a pollutant gas (U.S. EIA, 2009). In other words, the minor emission from

industrial sources has an extreme effect on global warming. In this paper, I present hydrate-based gas separation (HBGS) technology, one of the measures of GHG control.

1.1.2 Gas Hydrate

Gas hydrates are defined as crystalline compounds that are formed when the host water and guest molecules physically interact. Three types of hydrate structures are well-known: structure I (sI), structure II (sII), and structure H (sH) as shown in Figure 1. This classification is derived from the differences in the crystal structure as well as the cage shape and size of the gas hydrate (Sloan, 1988; Sloan, 2003, Sloan, 1998; Makogon et al., 2007). Figure 2 shows the size of each cage encaging the guest molecules depends on the size ratio of the guest molecules to the cage, and causes guest molecules in the hydrate cages to be selectively enclathrated (Sloan, 1988; Kang & Lee, 2000). The crystalline unit of the cubic sI hydrate consists of two small 5^{12} and six large $5^{12}6^2$ cages, and that of the cubic sII hydrate has sixteen small 5^{12} and eight large $5^{12}6^4$ (Table 3) (Sloan, 1988). The hexagonal sH hydrate includes three types of cages: three 5^{12}, two $5^{12}6^4$, and a $4^35^66^3$. It requires large guest substances such as adamantine and methylcyclohexane with a smaller help gas for cage stability (Udachin et al., 2002; Ripmeester et al., 1987). As the amount of world energy use continuously increases, it can be predicted that GHG emission as well as GHG concentration in the atmosphere will also increase. Therefore, studies in the past several decades have focused on HBGS technology (Kang & Lee, 2000; Linga et al., 2007; Linga et al., 2007; Xu & Li, 2014). Several different guest molecules in gas phases such as methane and carbon dioxide can be trapped in a hydrate structure. Accordingly, researchers have considered gas hydrates as one of the most suitable applications of gas

storage and separation in the energy and environmental fields (Sloan, 1988; Kang & Lee, 2000; Linga et al., 2007; Linga et al., 2007; Xu & Li, 2014; Gudmundsson et al., 1994; Sun et al., 2003).

1.2. Purpose

HBGS technology is based on the characteristic of gas hydrate, the selective enclathration depending on the guest molecules. N_2O molecules are known to form sI hydrate, occupying both the small (5^{12}) and large ($5^{12}6^2$) cages of the sI hydrate framework. Although there have been several fundamental studies on the N_2O hydrate (Villard, 1888; Villard, 1897; Tammann & Krige, 1925; Mohammadi & Richon, 2009; Sugahara et al., 2009), the structural identification and cage occupancy of N_2O hydrate have not fully been understood.

In this study, I examine the structural identification and cage occupancies for N_2O-N_2 binary gas hydrates. Powder X-ray diffraction (XRD) and Raman spectroscopy are used to identify the crystal structure and to observe the behavior of guests occupied in the cages of hydrate structures. A thermodynamic model is used for the estimation of cage occupancies in small and large cages of N_2O-N_2 binary sI hydrates. To investigate guest release behavior and the corresponding self-preservation of guest in the pure N_2O hydrate and the N_2O/N_2 (40/60) binary gas hydrate, temperature-dependent Raman spectra are conducted. The phase equilibrium conditions of N_2O/N_2 (100/0, 80/20, 60/40, 40/60, 20/80) binary gas hydrates are measured. After the gas hydrate is completely formed, I investigate the initial concentration of gas mixtures and the final concentration of the dissociated hydrate in vapor phase. Lastly, I perform gas storage capacity analysis of pure N_2O hydrate with 2.5 MPa pressure and N_2O/N_2 (80/20, 60/40, 40/60, 20/80) binary gas hydrates with 3.5 MPa pressure.

Table. 1 GWP and CO_2-equivalent emissions of Greenhouse gases (IPCC, 2007).

Greenhouse gas	GWPs[a]	CO_2-equivalent emissions
CO_2	1	81
CH_4	21	7
N_2O	310	9
HFCs[1)]	1,300	x[b]
PFCs[2)]	7,000	x[b]
SF_6	23,900	x[b]

Table. 2 Global N_2O emissions (Perez-Ramirez et al., 2003).

Source	Emission amounts (Mt/y)
·Natural	ca.13
Soils	10
Oceans	2.9
Atmospheric chemistry	0.2
·Anthropogenic	ca.7
Agriculture	3.5
Industrial (Nitic/Adic acid production)	0.5
Fossil-fuel combustion	0.6~1.4
Biomass combusion	1.0
Sewage treatment	1.5
·ToTal	ca.20

1) HFCs : hydrofluorocarbons.
2) PFCs : perfluorocarbons.
[a]For a 100-year time horizon.
[b]3% for all halogenated compounds including the HFCs, PFCs and SF_6.

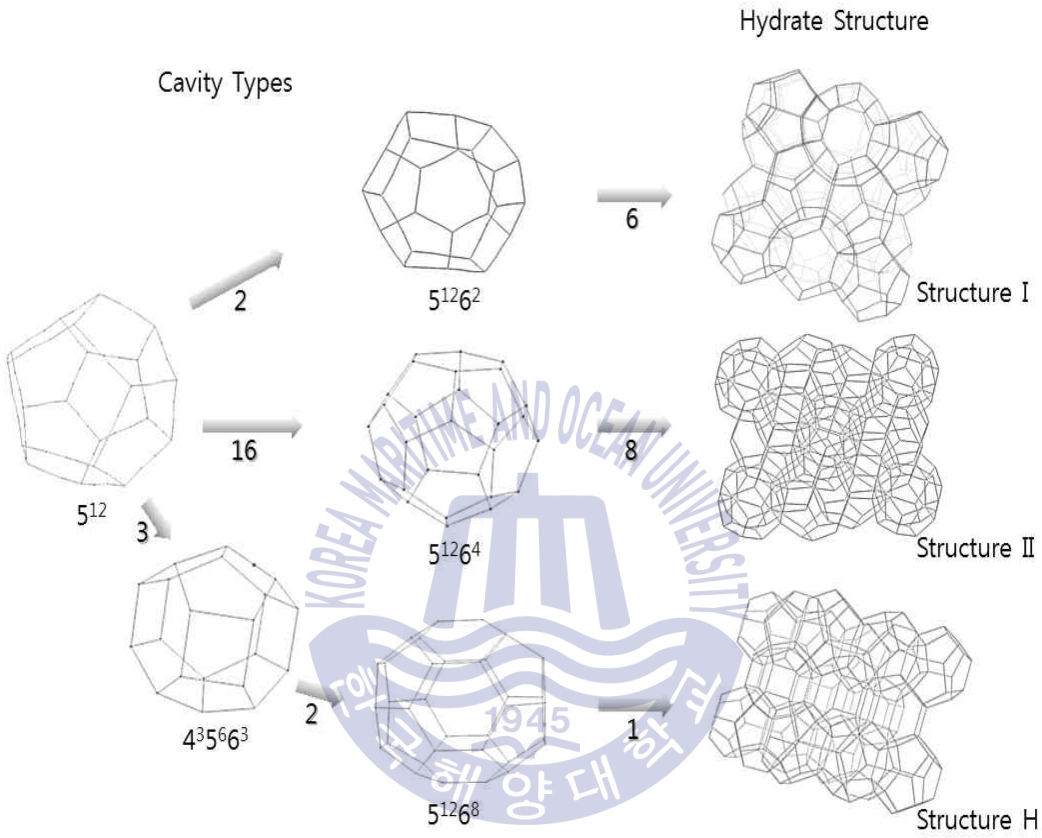

Figure. 1 Clathrate hydrate types and guest molecules.

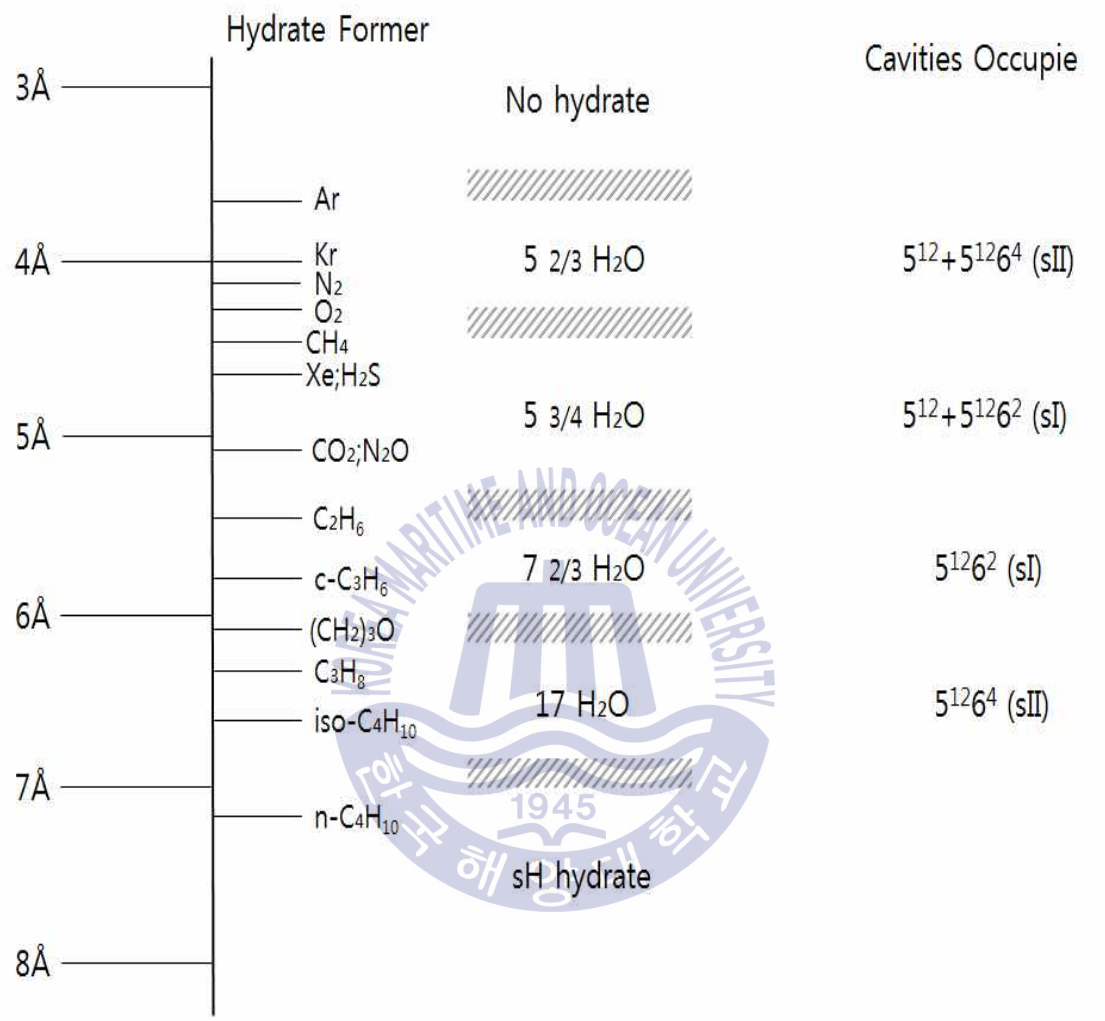

Figure. 2 Guest molecules and cavities occupied a simple hydrate.

Table. 3 Hydrate structure characteristics (Sloan 1988).

Hydrate Crystal Structure	**I**		**II**	
Crystal Type	cubic		cubic	
Space Group	*Pm3n*		*Pm3n*	
Lattice Parameters	a = 12		a = 17.3	
Cavity	small	Large	Small	Large
Description	5^{12}	$5^{12}6^2$	5^{12}	$5^{12}6^4$
Number of Cavities	2	6	16	8
Average Cavity Radius,	3.95	4.33	3.91	4.73
Coordination Number	20	24	20	28
Idea gas composition	$6X \cdot 2Y \cdot 46H_2O$		$8X \cdot 16Y \cdot 136H_2O$	

Chapter 2. Experimental Section

2.1. Materials

N_2O with a purity of 99.99 mol% and N_2O/N_2 (100/0, 80/20, 60/40, 40/60, 20/80) was provided by Kyongdong Gas Co. (South Korea). THF with a purity of 99.9 mol% was obtained from Sigma-Aldrich Inc. Deionized water was supplied from a Millipore purification unit. All sample of N_2O-N_2 binary gas hydrates were prepared as can be seen in Figure 3.

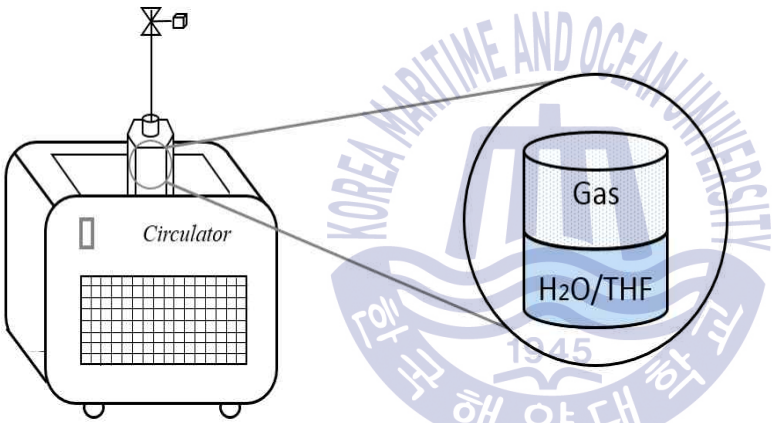

Pure N_2O	N_2O+THF 5.56 mol%	N_2O/N_2 mixed (80/20, 60/40, 40/60, 20/80)
N_2O - 268K, 25bar	N_2O - 268K, 25bar	N_2O/N_2 - 268K, 35bar
100μm powdered Ice	100μm powdered H_2O - 72g(4 mol) THF – 16.981g(5.56 mol%)	100μm powdered Ice

Figure. 3 Experiment conditions for samples

2.2. Experimental Procedure

The experiment design diagram was presented in Figure 4. First of all, the equilibrium conditions of the N_2O-N_2 binary gas hydrates were measured using a high-pressure equilibrium cell with two tempered glasses on opposite sides for watching the hydrate formation process and a magnetic driver for mixing. The equilibrium cell was placed in a liquid bath with a thermometer with a resolution of 0.1 K and a pressure gauge with a resolution of 0.01 MPa to determine the system temperature and pressure. The equilibrium cell (250 cm^3) was charged with 80 cm^3 of deionized water and pressurized to the desired pressure with N_2O-N_2 mixture gas. When the cell condition was stabilized, hydrate formation began after cooling the cell. After completion of the hydrate formation, the gas hydrate was slowly dissociated by increasing the system temperature with a stepwise rate of 0.1 K/hr. I verified and measured the equilibrium point by the naked eye as well as by computer system throughout the whole experiment to confirm the three phase (H-Lw-V) conditions and to capture the exact moment that the minute hydrate crystals in the liquid phase were completely dissociated (Figure 5).

For the formation of N_2O-N_2 binary gas hydrates, I carried out the following procedure. The deionized water was frozen at 269 K for a day and then ground to a fine powder with a 100 μm sieve. A hexagonal cell (20 cm^3) was prepared and filled with ground powder and five stainless steel balls. It was pressurized to 2.5 MPa for pure N_2O hydrate and 3.5 MPa for N_2O/N_2 (80/20, 60/40, 40/60) binary gas hydrates and 4.5 MPa for the N_2O/N_2 (20/80) binary gas hydrate. The liquefaction of pure N_2O can occur at the pressure of 2.7 MPa and temperature of 268 K conditions, and thus; pure N_2O hydrate sample was pressurized to 2.5 MPa. For spectroscopic analysis, precise results were required. However, From our

experimental results, the N_2O/N_2 (20/80) binary gas hydrate was rarely formed under a pressure of 3.5 MPa at 268K. Thus, the pressure for the N_2O/N_2 (20/80) binary gas hydrate was increased to 4.5 MPa for definite spectroscopic analysis. I placed the cell in a liquid bath of 268 K and shook the cell in order to mix the hydrate sample every three hours. Mixing was verified aurally by listening for the sound of colliding metal balls. During the formation of the gas hydrate, the pressure was dropped and I then filled the cell with the desired pressure again for about a week. When the hydrate formation was completed, the cell was immediately immersed in liquid nitrogen (LN2). The formed hydrate sample was used for structural analysis by XRD (Figure 6) and Raman spectroscopy (Figure 7,8), for gas compositions by gas chromatography (Figure 9), and for gas storage by a measuring cylinder (Figure 10).

In this study, the initial concentration of gas mixtures and the final concentration of the gas phase in equilibrium with the hydrate phase were measured by gas chromatography (Younglin, ACME 6100). I used Raman spectroscopy with a single monochromator of 1800 grooves/mm and a multichannel air-cooled CCD detector. The excitation source was an Nd:YAG laser emitting a 532 nm line with a powder of 150 mW. The Raman spectroscopic measurements for the N_2O–N_2 binary gas hydrates were performed under liquid argon instead of LN2 while using a microscope stage (Linkam, THMS 600 model) to prevent nitrogen in the hydrate phase from being disturbed by nitrogen in the air at ambient pressure. For temperature-dependent Raman measurement, the sample temperature on the microscope stage was changed from 162 K to 273 K at intervals of 3 K for pure N_2O hydrate and from 155 K to 273 K at intervals of 5 K for N_2O/N_2 (40/60) binary gas hydrate, taking 10 minutes for each step to reach the desired temperature. Lastly, the crystalline structure of the binary gas hydrate

samples was investigated by XRD (RIGAKU D/ MAX-2500) with a wavelength of 1.54960 Å at the KAIST Analysis Center for Research Advancement (KARA). All XRD measurements were conducted at 100 K and in the range of 5-40° with a step size of 0.02°. More detailed information on the experimental setup could be found in our previous studies (Lee et al., 2012; Shin et al., 2009).

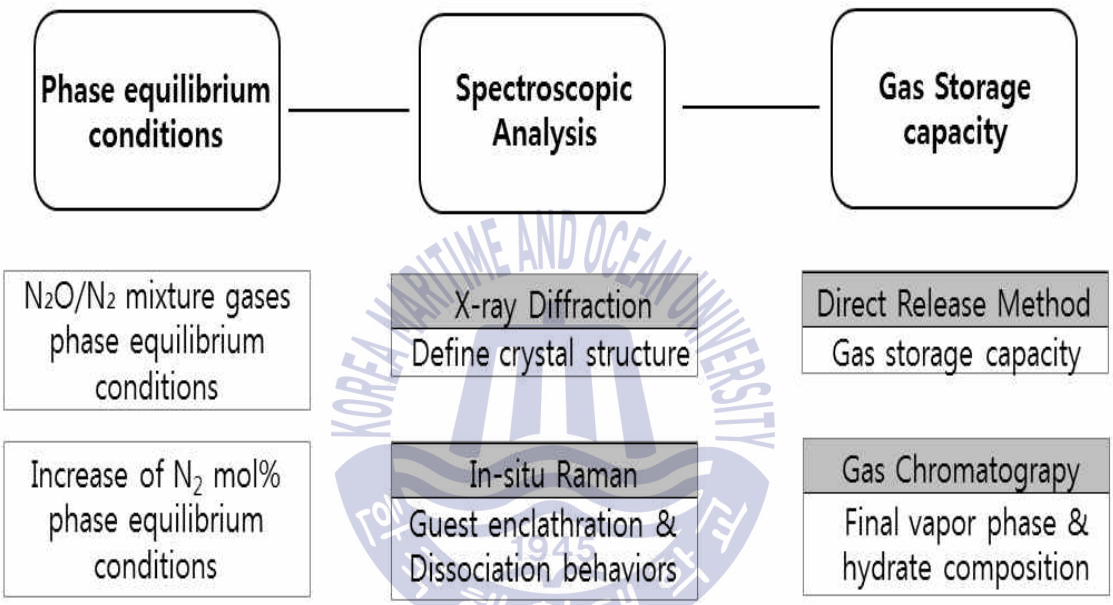

Figure. 4 Experiment design diagram.

2.3. Method of Analysis

2.3.1. Phase Equilibrium Conditions

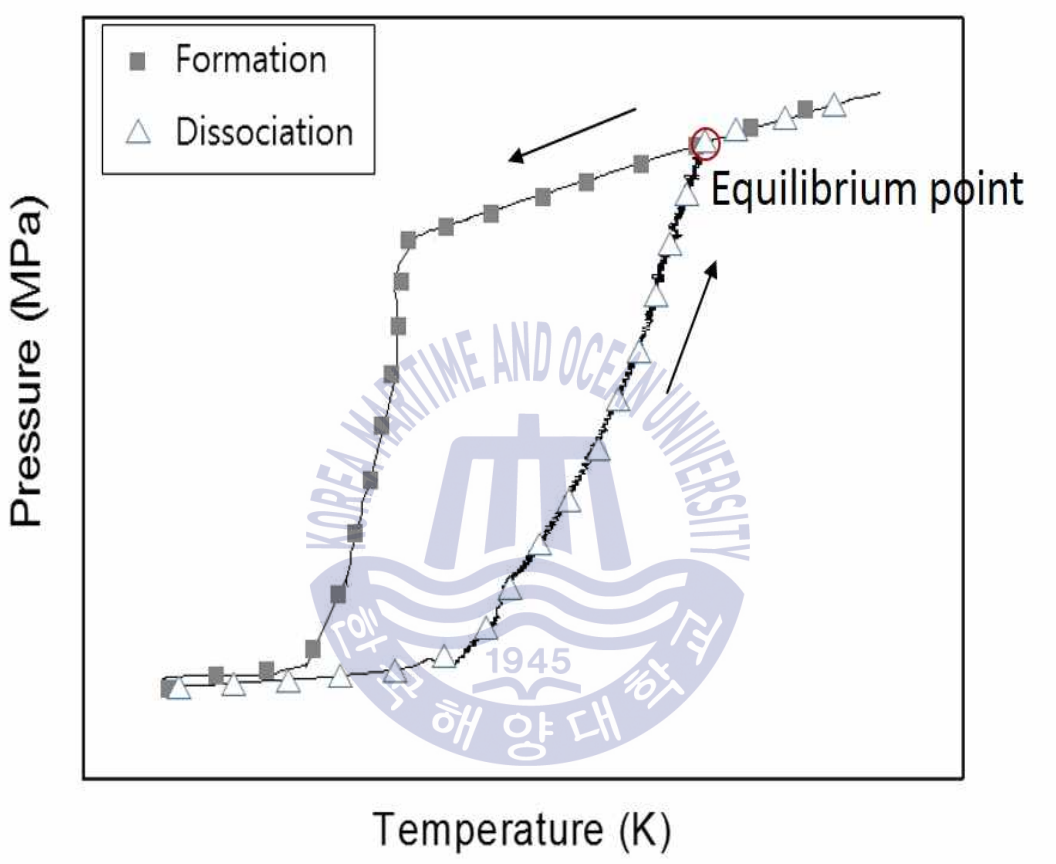

Figure. 5 Gas hydrate formation and dissociation graph.

2.3.2 X-ray Diffraction

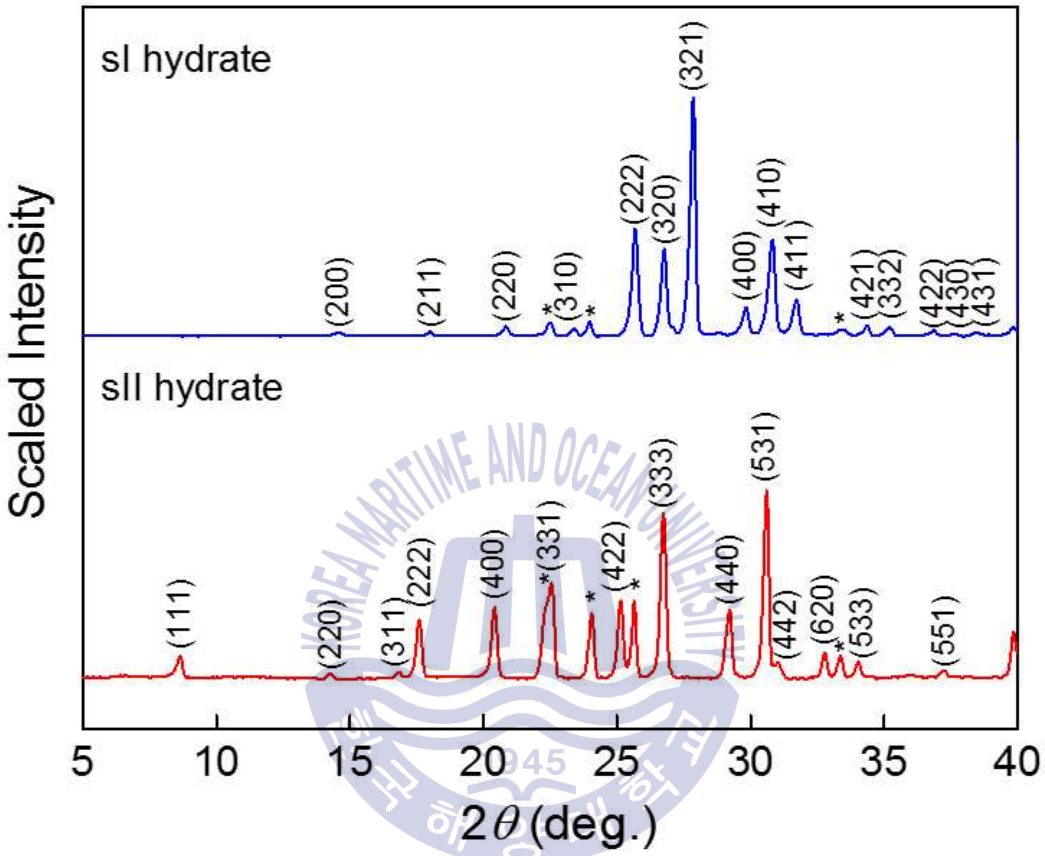

Figure. 6 X-Ray Diffraction data for sI and sII hydrate.

2.3.3. Raman Spectroscopy

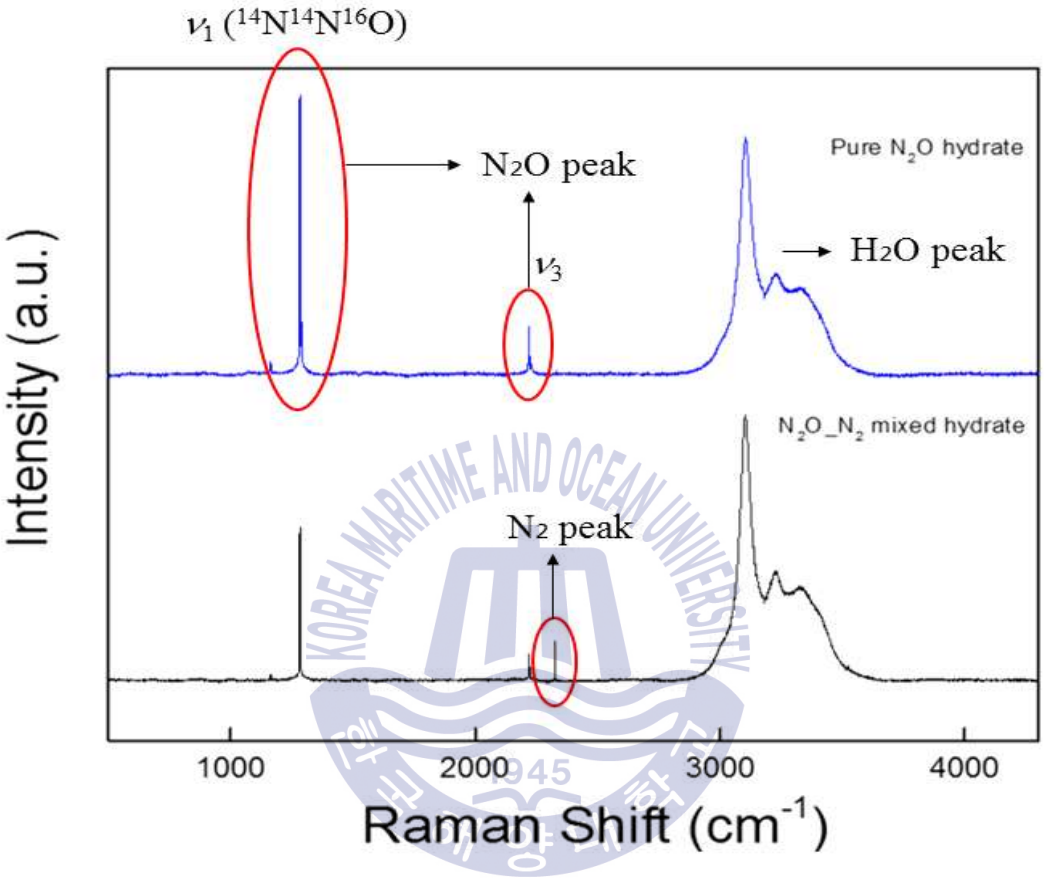

Figure. 7 Raman Spectroscopy data for N_2O and N_2 peak.

2.3.4. Cage Occupancy

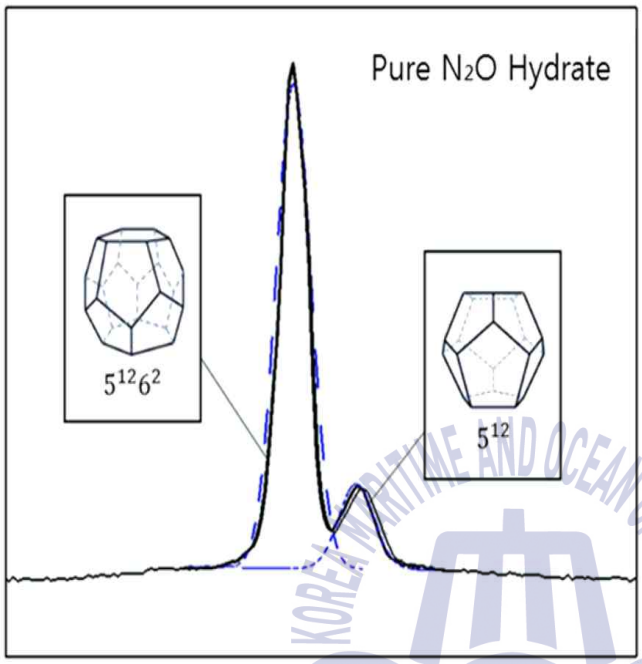

$$A_{(L)} : A_{(S)} = \frac{\theta_{(L)}}{3} : \theta_{(S)}$$

$$A_{(L)} : A_{(S)} = 5 : 1$$

$$\theta_{(L)} = \frac{5}{3}\theta_{(S)}$$

Figure. 8 Cage occupancy for the large and small cages from Raman data of pure N_2O hydrate.

2.3.5. Gas Selectivity

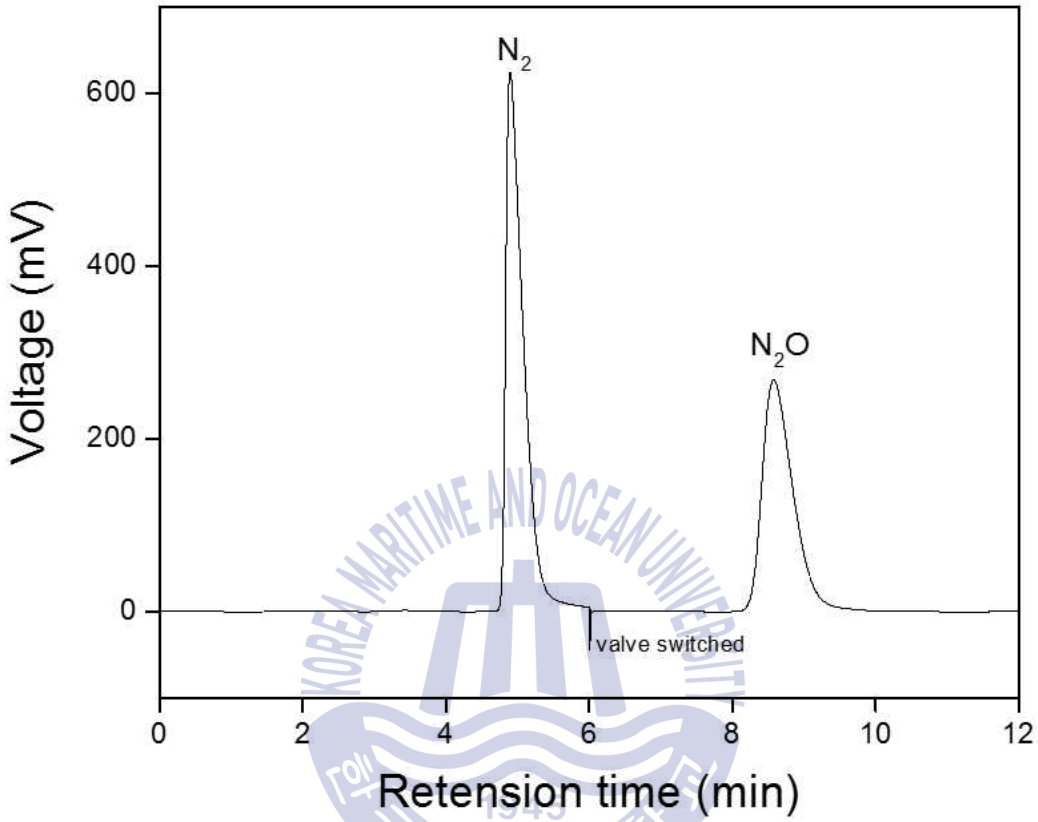

	area(mV*Sec)	area (%)	mole(%)
N_2	10546.1780	56.9583	67.1019
N_2O	7969.4498	43.0417	41.5891

Figure. 9 Gas Chromatography data from N_2O and N_2 mixed gas.

2.3.6 Gas Storage Capacity

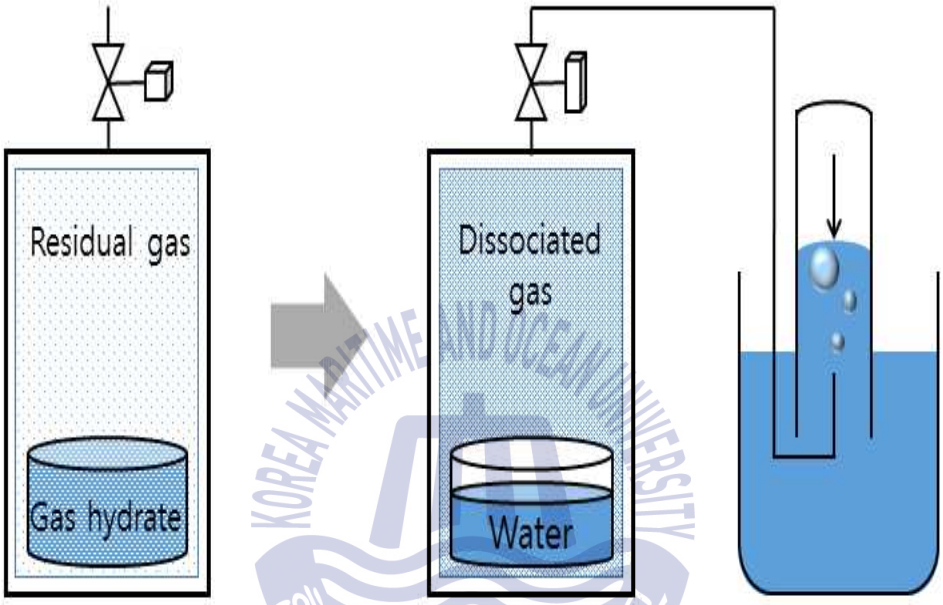

Figure. 10 Gas storage capacity measurement.

Chapter 3. Results and Discussion

3.1. XRD patterns

The crystal structure and guest enclathration of binary gas hydrates formed from N_2O and N_2 gas mixtures have been identified by powder X-ray diffraction (XRD) and Raman spectroscopy.

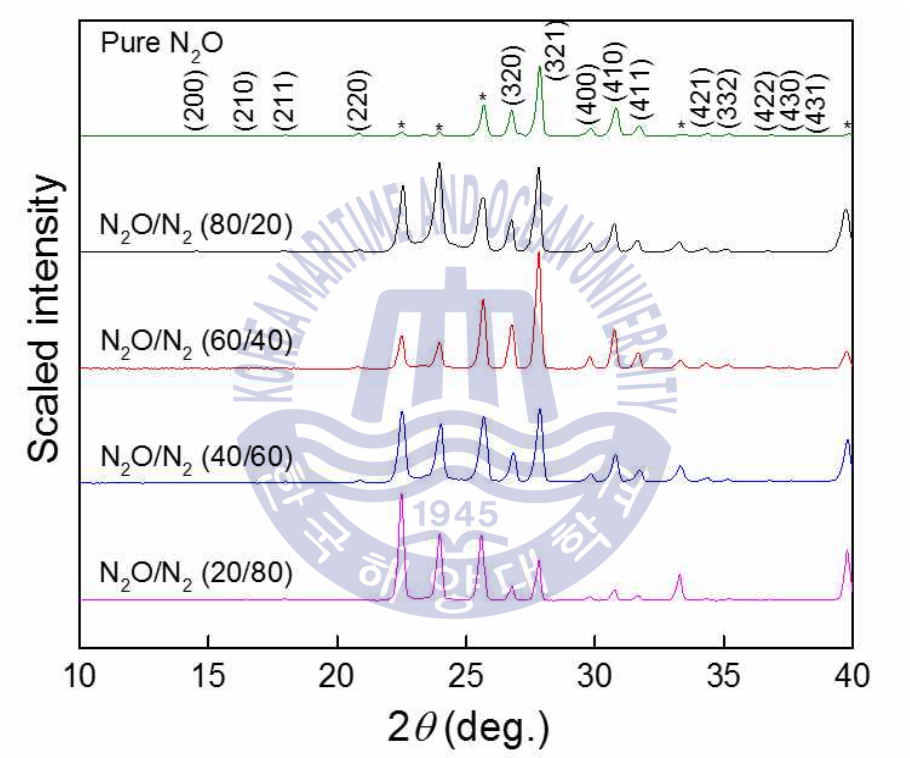

Figure. 11 XRD patterns of N_2O-N_2 binary gas hydrates. Asterisks denote the peaks for the hexagonal ice (Ih).

Figure 11 showed the XRD patterns of N_2O/N_2 (100/0, 80/20, 60/40, 40/60, 20/80) binary gas hydrates with the Miller indices. Some peaks with the asterisk (*) implied Bragg peaks corresponding to the hexagonal ice phase (Ih), and XRD results indicated that the crystal structures of all

N_2O-N_2 binary gas hydrates could be assigned as the structure I hydrate, having the cubic unit cell with a space group of *Pm3n*. The lattice parameter (Å) and the unit cell volume ($Å^3$) of all N_2O–N_2 binary gas hydrates were summarized in Table 4.

Table. 4 Crystal Structure, Lattice Parameter, and Unit Cell Volume of N_2O-N_2 Binary Gas Hydrates.

Hydrate	Structure	Space group	Lattice parameter (Å)	Unit cell volume ($Å^3$)
Pure N_2O	sI	*Pm3n*	a =11.9710	1715.50
N_2O/N_2(80/20)	sI	*Pm3n*	a =11.9691	1714.70
N_2O/N_2(60/40)	sI	*Pm3n*	a =11.9555	1713.98
N_2O/N_2(40/60)	sI	*Pm3n*	a =11.9500	1718.80
N_2O/N_2(20/80)	sI	*Pm3n*	a =11.9865	1728.03

3.2 Raman spectra

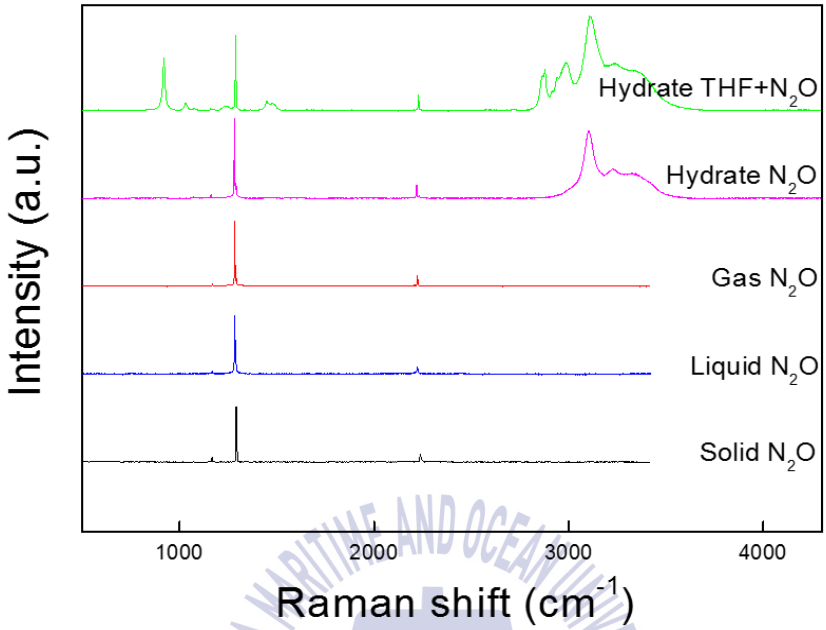

Figure. 12a Raman spectra of gaseous, liquid and solid N_2O and clathrate hydrates encapsulating N_2O molecules.

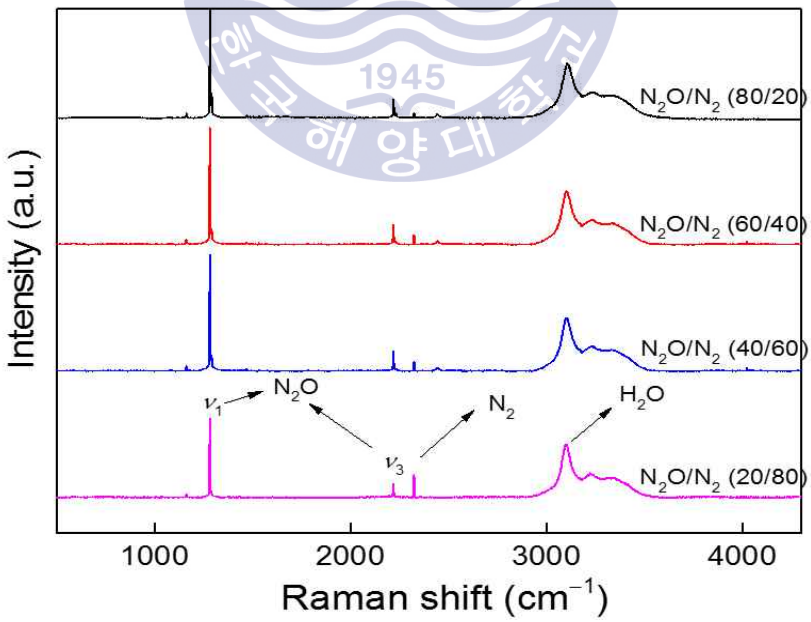

Figure. 12b Raman spectra of N_2O-N_2 binary gas hydrates. ν_1 and ν_3 are the N-O stretching vibration and the N-N stretching vibration, respectively.

Detailed information on the crystal structure and the guest inclusion behavior of N_2O hydrates was also provided by Raman spectroscopy. Figure 12 showed the Raman spectra of N_2O molecules in the gas, liquid, and solid phases and N_2O-N_2 binary gas hydrates and N_2O–THF hydrate. Figure 12a and 12b showed the wavenumbers of intra-molecular vibration for N_2O molecules in gas, liquid, solid, and hydrate phases, determined from the Raman spectra, were summarized in Table 5.

Table. 5 Vibration mode of N_2O molecules in gas, liquid, solid, and hydrates.

Assignment	Wavenumber(cm^{-1})				
	Gas (298K)	Liquid (298K)	Solid (140K)	sI hydrate (140K)	sII hydrate (140K)
ν_2	588.8[3]		588	585	582
$2\nu_2$(biphonon ν^-)	1169	1167	1166	1162	1158
$2\nu_2(\nu_2(k)+\nu_2(-k))$			1177		
$\nu_1(^{14}N^{14}N^{18}O)$			1253		
$\nu_1(^{15}N^{14}N^{16}O)$			1277		
$\nu_1(^{14}N^{14}N^{16}O)$	1285	1284	1291	1282[4], 1290[5]	1288[6]
ν_3	2223	2222	2237	2218[4], 2231[5]	2228[6]

3) Anderson & Sun, 「Raman spectra of molecular crystals. Carbon dioxide and nitrous oxide」, (1990), pp.539.
4) N_2O molecule in the large cages of sI hydrate.
5) N_2O molecule in the small cages of sI hydrate.
6) N_2O molecule in the small cages of sII hydrate.

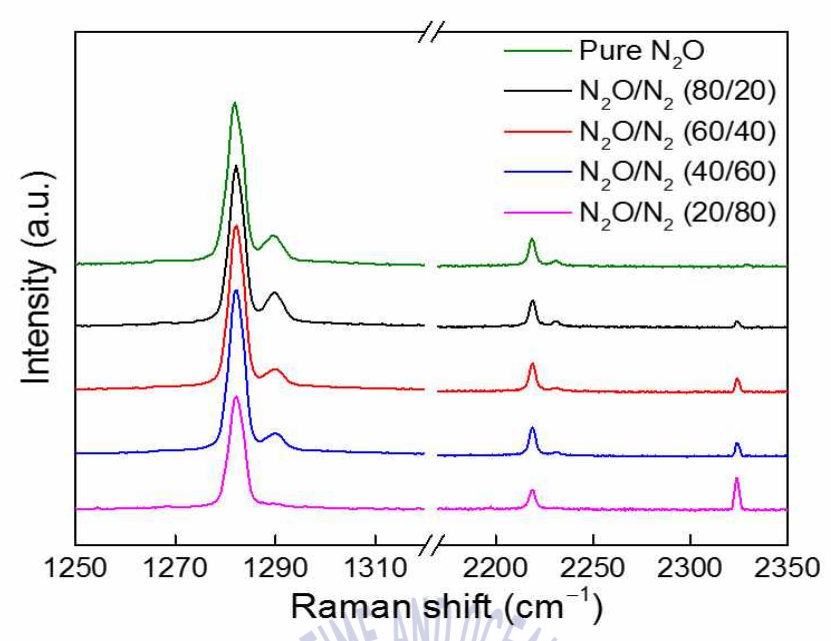

Figure. 12c Enlargement of the ν_1 and ν_3 spectral regions of N_2O and the N-N stretching vibration region of N_2.

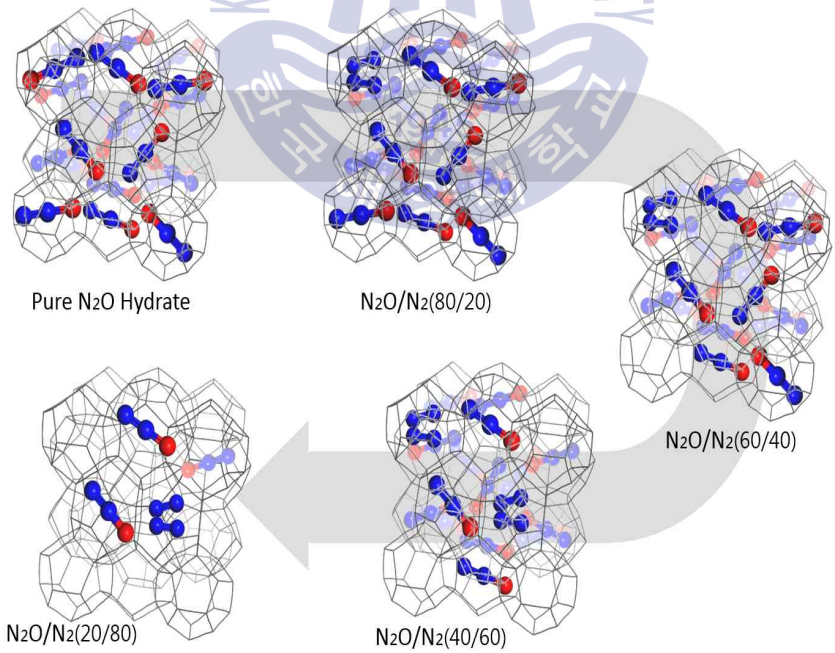

Figure. 12d Description of N_2O-N_2 binary gas hydrates as the concentration of N_2O decreases.

The enlargement of the ν_1 and ν_3 spectral regions of N_2O molecules and the N-N stretching vibration region of N_2 molecules was shown in Figure 12c. There were three Raman-active vibration modes of N_2O molecules: N−O stretching vibration (ν_1) at around 1280 cm^{-1}, and N−N−O bending vibration (ν_2), N−N stretching vibration (ν_3) at around 2230 cm^{-1} (Cahill & Lerol, 1969; Olijnyk et al., 1990; Anderson & Sun, 1971). For N_2O/N_2 (80/20) binary gas hydrate (black line in Figure 12b and 12c), two Raman band (1282 and 1290 cm^{-1}) were observed in the ν_1 spectral region, the strongest Raman band of N_2O as shown in Figure 12c. XRD results demonstrated all N_2O-N_2 binary gas hydrates formed sI hydrate under the desired equilibrium conditions. In other words, the dominant Raman band at 1282 cm^{-1} implied that N_2O molecules were occupied in the large $5^{12}6^2$ cages of the sI hydrate framework and the adjacent Raman band at 1290 cm^{-1} indicated N_2O molecules in the small 5^{12} cages of the sI hydrate, designated as ν_1 vibration mode (Yang et al., 2016). I could observe the same trends in N_2O/N_2 (60/40) and N_2O/N_2 (40/60) binary gas hydrates. However, for the N_2O/N_2 (20/80) binary gas hydrate, a single Raman band at 1282 cm^{-1} was revealed in the same ν_1 vibration, indicating that N_2O molecules occupied only the large $5^{12}6^2$ cages of the sI hydrate framework. Likewise, in the ν_3 spectral region for the N−N stretching vibration, two Raman bands, relatively weak spectra, were observed at 2218 and 2231 cm^{-1} in all samples except N_2O/N_2 (20/80) binary gas hydrate. It indicated the inclusion of N_2O molecules in both small and large cages of sI hydrates. On the other hand, the sample of N_2O/N_2 (20/80) binary gas hydrate had a single Raman band at 2218 cm^{-1}, implying that the encapsulation of N_2O molecules only in large cages of sI hydrate. From the Raman spectra of N_2O in the wavenumber range of ν_1 and ν_3, I could observe the preferential occupation of N_2O molecules in the large cages of sI hydrates. The Raman peak at 2324 cm^{-1} could be assigned as the N−N stretching vibration of N_2 molecules occupied in the sI hydrate. Figure 12d described the N_2O-N_2 binary gas hydrates as the concentration of N_2O decreased.

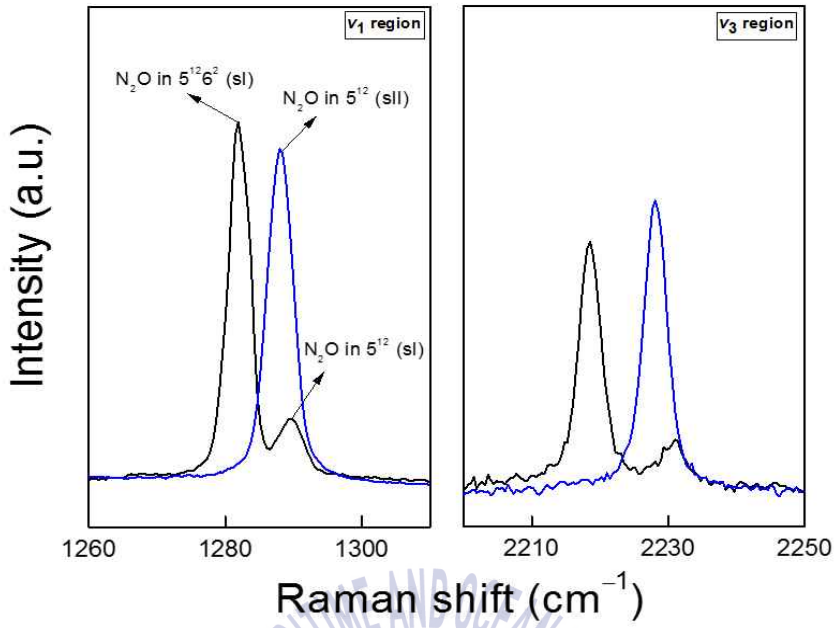

Figure. 13a Enlargement of Raman spectra in the ν_1 and ν_3 region of N_2O encaged in pure N_2O (sI) hydrate (black line) and N_2O-THF (sII) hydrate (blue line).

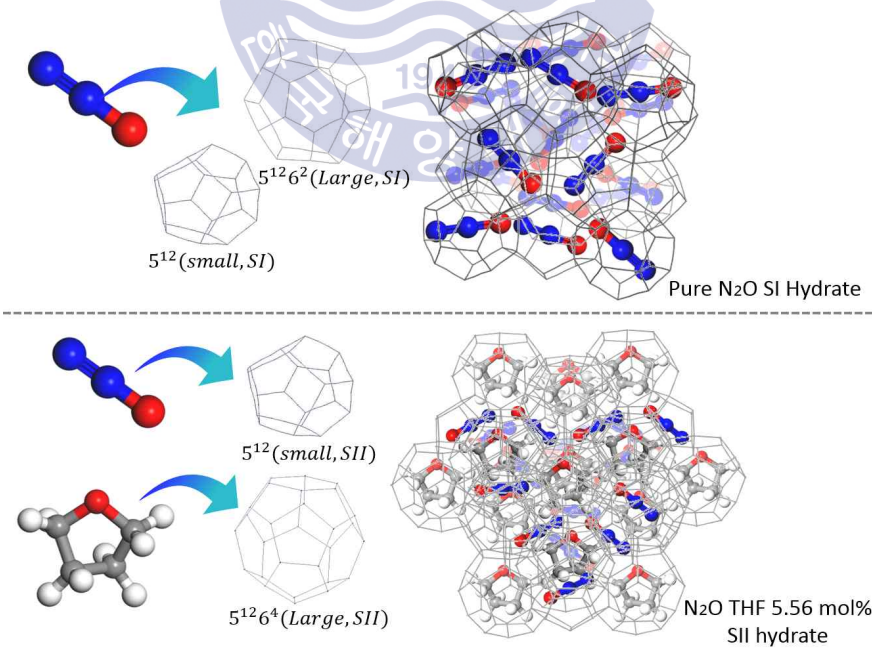

Figure. 13b Description of N_2O sI and N_2O-THF sII hydrate.

For pure N_2O hydrate, two Raman bands in the ν_1 spectral region were measured at 1282 and 1290 cm^{-1} (Figure 13a). From the XRD results, the crystal structure of pure N_2O hydrate was identified as sI hydrate. Thus, the prominent Raman band at 1282 cm^{-1} could be attributed to N_2O molecules encaged in the large $5^{12}6^2$ cages of the sI hydrate framework, while the relatively small Raman band at 1290 cm^{-1} can be assigned as the ν_1 vibration mode of N_2O molecules encaged in the small 5^{12} cages. However, a single Raman peak was observed at 1288 cm^{-1} in the ν_1 spectral region for N_2O−THF hydrate, indicating that N_2O molecules were occupied only in the small 5^{12} cages of sII hydrate and the large $5^{12}6^4$ cages of sII hydrate were fully occupied by THF molecules. Figure 13b described pure N_2O sI hydrate and N_2O−THF 5.56 mol% sII hydrate.

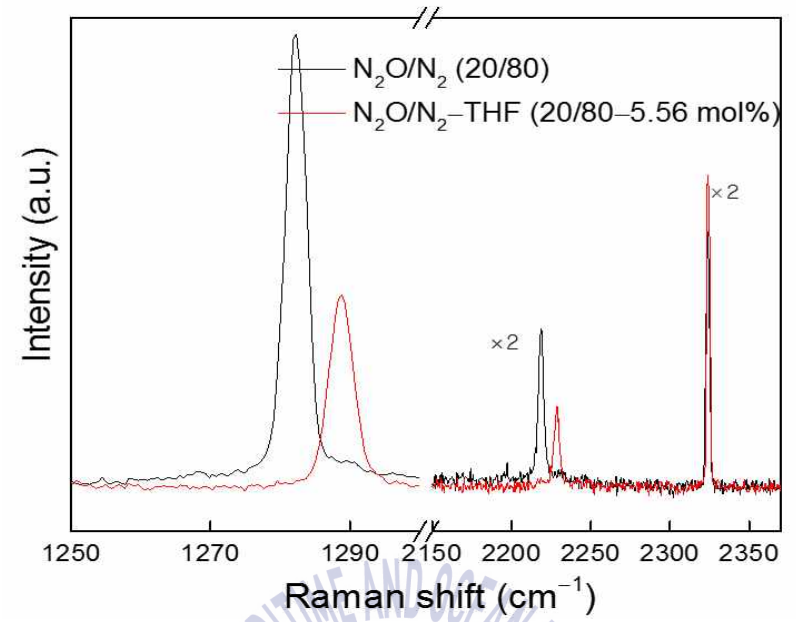

Figure. 14a Raman spectra of N_2O/N_2(20/80) binary gas hydrate and N_2O/N_2(20/80)-THF 5.56 mol% ternary clathrate.

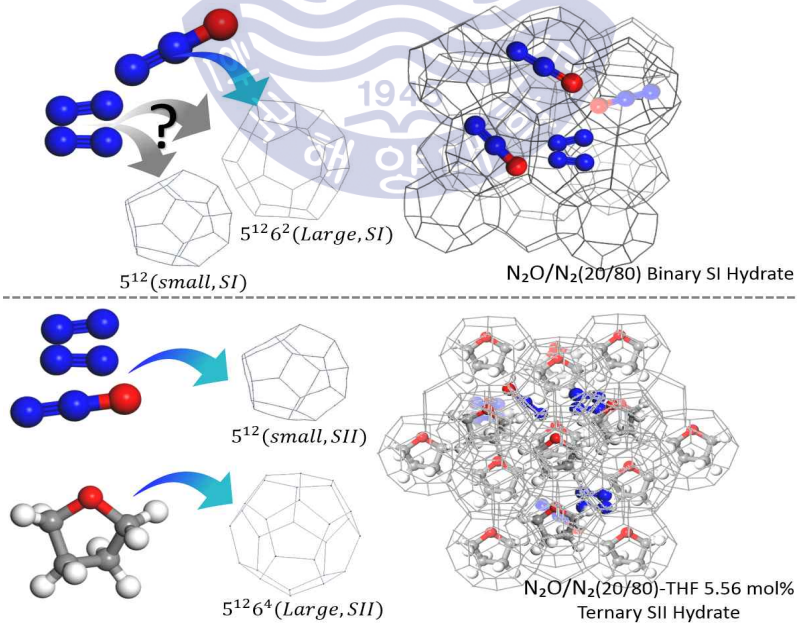

Figure. 14b Description of N_2O/N_2(20/80) sI and N_2O/N_2 (20/80)−THF sII hydrate.

Furthermore, I analyzed Raman signals of pure N_2O and N_2O/N_2 (20/80) gas hydrates in the presence of THF (Tetrahydrofuran) 5.56 mol% to check the Raman signal differences of N_2O molecules for different hydrate structure, described in Figure 14. THF is well-known sII hydrate former, occupying the large cages of sII hydrate with almost full occupancy. Thus, a single Raman peak was observed at 1288 cm^{-1} in the ν_1 spectral region for N_2O−THF 5.56 mol% hydrate, indicating that N_2O molecules were occupied only in the small 5^{12} cages of sII hydrate and the large $5^{12}6^4$ cages of sII hydrate were fully occupied by THF molecules. N_2O and N_2 molecules in N_2O/N_2 (20/80) gas hydrate in the presence of THF 5.56 mol% were expected to be captured in the small cages of sII hydrate (Figure 14a). A single Raman band of N_2O at 1282 cm^{-1} in the ν_1 spectral region and at 2218 cm^{-1} in the ν_3 spectral region for N_2O/N_2 (20/80) binary gas hydrate was observed, indicating the inclusion of N_2O molecules in the large cages of sI hydrate, whereas a single Raman band of N_2O at 1288 cm^{-1} in the ν_1 spectral region and at 2228 cm^{-1} in the ν_3 spectral region, implying that the enclathration of N_2O molecules in the small cages of sII hydrate for N_2O/N_2 (20/80) gas hydrate in the presence of THF 5.56 mol% was observed. For the Raman band at around 2324 cm^{-1}, it should be noted that the difference in Raman signal of N_2 molecules from the small cages of sI or sII hydrates was not identified as shown in Figure 14b (Sasaki et al., 2003). Figure 14b described N_2O/N_2 (20/80) sI hydrate and N_2O/N_2 (20/80)−THF sII hydrate.

3.3 Raman Spectra of the Vibration Modes

In the overtone ($2\nu_2$) spectral region, the Raman bands of N_2O molecules were observed in a wavenumber range of 1158-1169 cm^{-1} (Table 5 and Figure 12). The Raman spectra of N_2O molecules showed the Fermi resonance between the ν_1 vibration and overtone $2\nu_2$, which was weaker than for CO_2 (Anderson and Sun, 1971). A broad and less intense Raman band observed at 1177 cm^{-1} for solid N_2O was assigned to the [ν_2 (k) + ν_2 (-k)], which was caused by the an-harmonic coupling of the fundamental ν_1 and the two-phonon continuum. For all the samples shown in Figure 12c, the Raman bands for the N-N stretching vibration were observed around 2220 cm^{-1} in the ν_3 spectral region. In particular, two Raman bands of N_2O/N_2 (100/0, 80/20, 60/40, 40/60) hydrates were also observed at 1282 and 1290 cm^{-1} (ν_1) and 2218 and 2231 cm^{-1} (ν_3), respectively. It implied that the Raman band at 1282 (ν_1) and 2218 (ν_3) cm^{-1} indicated the inclusion of N_2O molecules in the large cages of the sI hydrate, and the relatively small Raman band at 1290 (ν_1) and 2231 (ν_3) cm^{-1} represented the inclusion of N_2O molecules in the small cages of the sI hydrate. For N_2O/N_2 (20/80) binary gas hydrate, a single Raman band at 1282 cm^{-1} (ν_1) and 2218 cm^{-1} (ν_3) was revealed, indicating encapsulation of N_2O molecules occupied only the large $5^{12}6^2$ cages of the sI hydrate framework. However, a single Raman band was observed at 1288 cm^{-1} (ν_1) and 2228 cm^{-1} (ν_3), indicating that N_2O molecules occupied the small 5^{12} cages of the sII hydrate for N_2O−THF hydrate.

3.4 Cage Occupancy

The fractional occupancy ratio (θ_S/θ_L) of N_2O trapped in the small 5^{12} cages and large $5^{12}6^2$ cages of N_2O/N_2 (100/0, 80/20, 60/40, 40/60, 20/80) binary gas hydrates were estimated by using the peak area ratio (A_L/A_S) of N_2O molecules from the experimental data (Raman spectroscopy shown in Figure 12), implying the relative ratio of the large to small cages of N_2O molecules. The Raman peak ratio in the ν_1 spectral region (Figure 12c) was used to estimate the occupancy of N_2O molecules in hydrate cages. For pure N_2O hydrate, Raman spectroscopy results revealed that the peak area ratio (A_L/A_S) of N_2O molecules in the large cages relative to those in the small cages was $\approx$ 5. The chemical potential difference of water, μ^0, between filled hydrate and hypothetical empty hydrate was generally provided from statistical mechanics in the van der Walls and Platteeuw model; (van der Walls and Platteeuw, 1959)

$$\frac{\Delta\mu_w^0}{T} = \frac{3}{23} ln(1-\theta\ ) + \frac{1}{23} ln(1-\theta_S) \qquad (1)$$

where θ_L and θ_S were the fractional occupancies of guest (N_2O) molecules in the sI hydrate cages, leading to $\theta_L/\theta_S = A_L/3A_S$. From the Raman results and the value of $\Delta\mu_w^0$, (Sloan, 1988), I calculated that the large cage occupancy of N_2O in sI hydrate (θ_L) was 0.977 and the small cage occupancy of N_2O in sI hydrate (θ_S) was 0.586. In other words, N_2O molecules occupied approximately 98 percent of the large cages and 59 percent of the small cages in the sI clathrate hydrate. This also indicated that N_2O molecules primarily occupied the large cages rather than the small cages. As a hydrate number *n* is the ratio of the number of water molecules

to guest molecules in the hydrate structure, the hydrate number for pure N_2O hydrate was $n \approx 6.5$, which was higher than CH_4 hydrate ($\approx$ 6.0) and CO_2 hydrate ($\approx$ 6.2) (Lee et al., 2012).

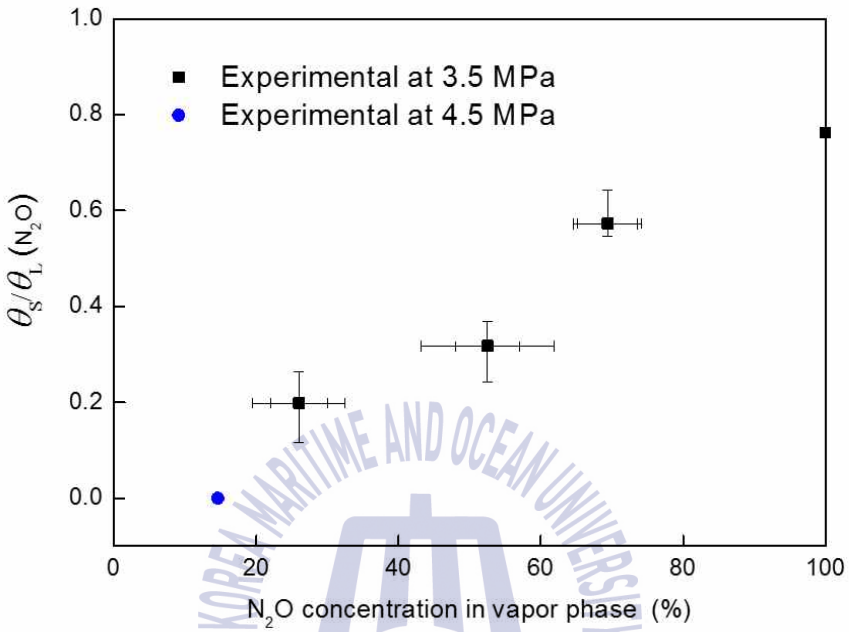

Figure. 15 Fractional occupancy ratio (θ_L/θ_S) of N_2O encaged in N_2O-N_2 binary gas hydrates as a function of N_2O concentration in vapor phase at 268K.

In addition, I also investigated the fractional occupancy ratio (θ_S/θ_L) of N_2O in hydrate phase as a function of the N_2O concentration in vapor phase at temperature of 268 K and at dissociation pressures of 3.5 MPa and 4.5 MPa, and the results were shown in Figure 15. Even though the high-pressure reactors containing N_2O/N_2 (initial vapor composition: 80/20, 60/40, 40/60, 20/80) binary gas hydrates were re-charged to desired pressure conditions during hydrate formation, the final vapor composition was changed into 70/30, 55/45, 25/75, and 15/85, respectively, due to the preferential occupation of N_2O in hydrate phases. The fractional occupancy ratio (θ_S/θ_L) of N_2O in hydrate phase increaseed as the equilibrium

pressures as well as the concentration of N_2O in vapor phase increased

3.5 Hydrate Phase Equilibria

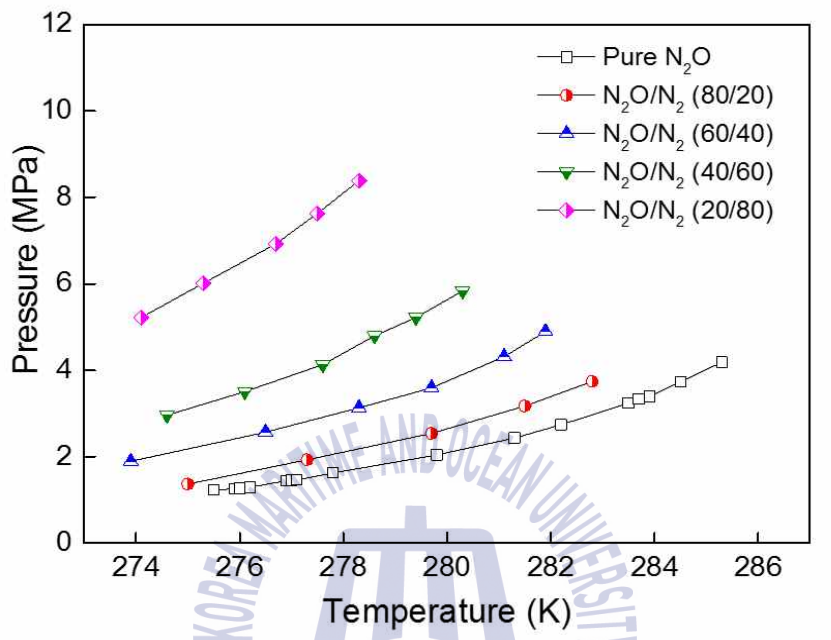

Figure. 16 Equilibrium dissociation pressures of N_2O-N_2 binary gas hydrates as a function of temperature.

Figure 16 shows the phase equilibrium conditions of N_2O/N_2 (100/0, 80/20, 60/40, 40/60, 20/80) binary gas hydrates in the temperature range of 274−286 K and the pressure up to 8.4 MPa (Yang et al., 2016). With the increase of N_2 concentration from 0 to 80 mol% in vapor phase, the three-phase equilibrium (H-Lw-V) of N_2O-N_2 binary gas hydrate were shifted into higher pressure and lower temperature conditions.

3.6 Temperature-dependent Raman Spectra

The effect of temperature on the dissociation behavior of pure N_2O hydrate and N_2O/N_2 (40/60) binary gas hydrate was investigated by temperature-dependent Raman spectra.

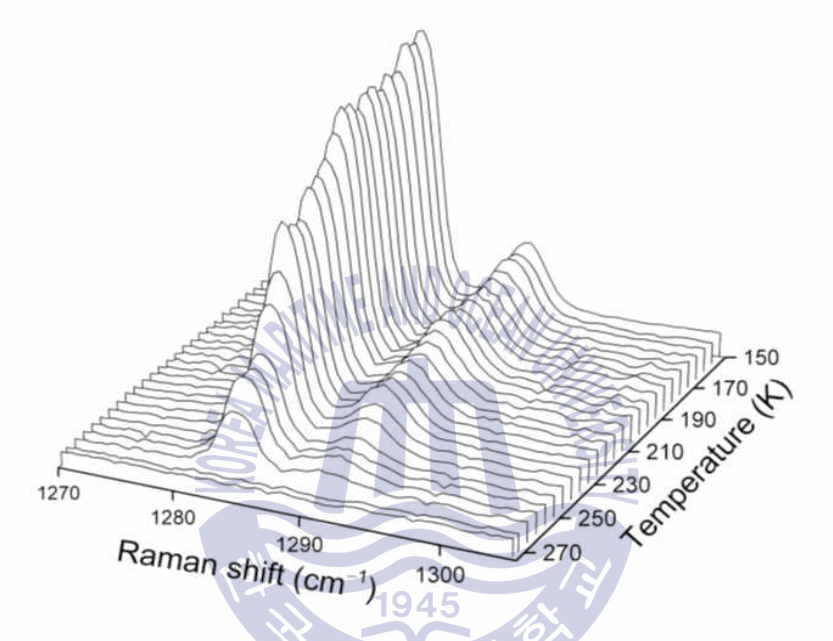

Figure. 17a Temperature-dependent Raman spectra of N_2O molecules trapped in pure N_2O hydrate.

Raman spectra for pure N_2O hydrate and were measured at ambient pressure and each specified constant temperature in the range of 150-273 K with 5 K intervals. The Raman peaks in the spectral ν_1 region of N_2O were normalized with the dominant Raman band at ~3100 cm^{-1} in the O-H vibration region of water (Figure 17a).

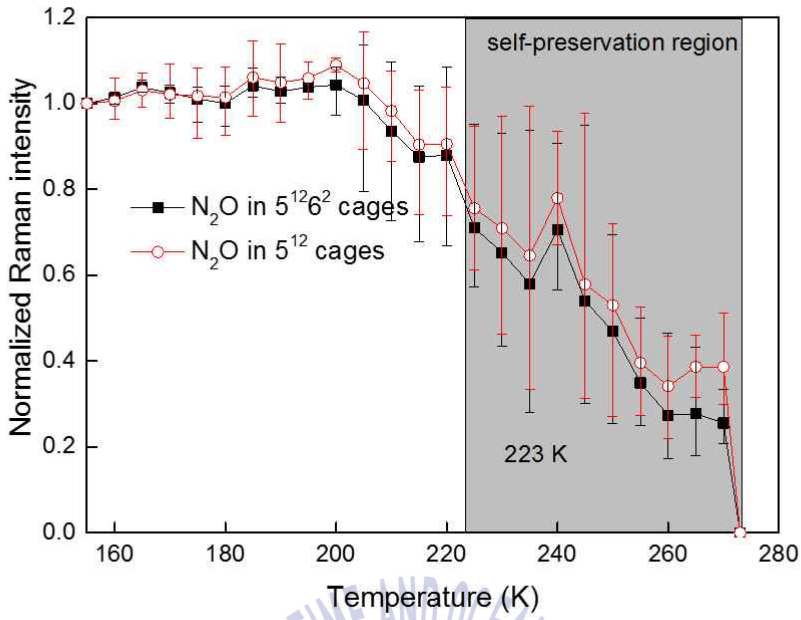

Figure. 17b Normalized relative intensity of Raman peaks for N_2O molecules trapped in large ($5^{12}6^2$) and small (5^{12}) cages of pure N_2O (sI) hydrate.

Figure 17b represented the relative change as a function of temperature in the Raman intensity of N_2O in the large $5^{12}6^2$ and small 5^{12} and cages of the N_2O sI hydrate. It could be likely the N_2O hydrate began to dissociate at around 200 K. The amounts of dissociated-hydrates increased as increasing temperature up to 230 K. However, the dissociation rate decreased at around 235 K, and then increases again at temperatures higher than 240 K. At 260 K, the remaining amount of N_2O hydrate was about 20-40 %, even though the condition was beyond the stability boundary. This was attributed to the self-preservation effect of pure N_2O hydrate. The self-preservation behavior of gas hydrate was known as the existence of abnormal hydrate stability in the temperature range of 240–270 K due to the formation of thin ice film emergence on gas hydrate surface.

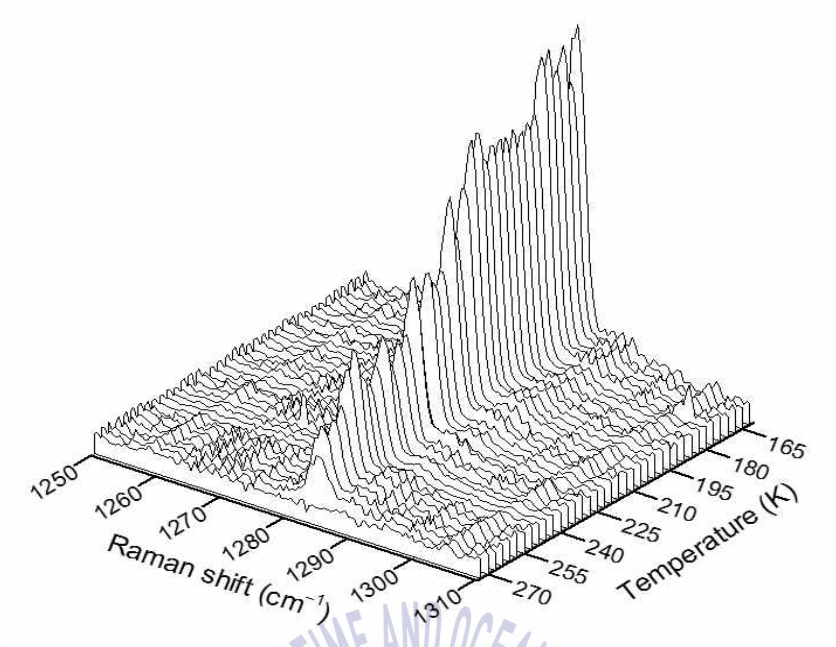

Figure. 17c Temperature-dependent Raman spectra of N_2O/N_2 (40/60) binary gas hydrate **(a)** ν_1 spectral region of N_2O.

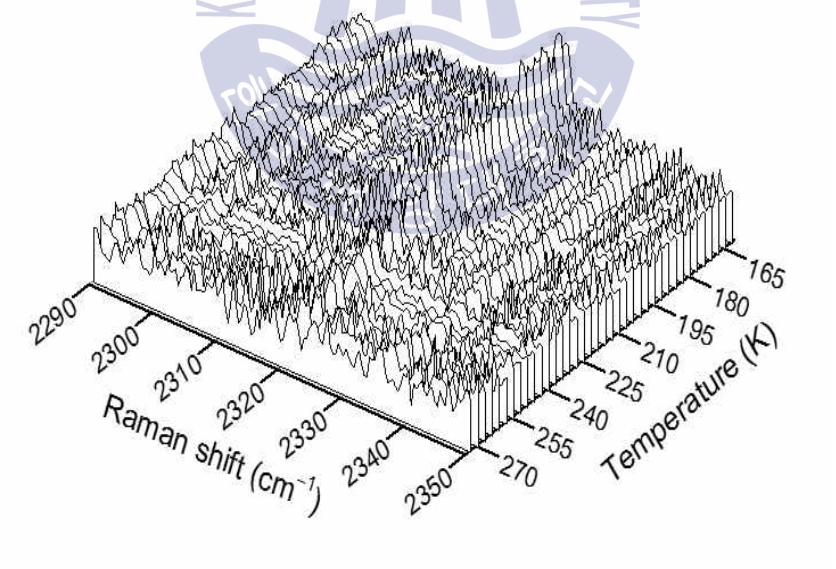

Figure. 17c Temperature-dependent Raman spectra of N_2O/N_2 (40/60) binary gas hydrate **(b)** N-N stretching vibration of N_2.

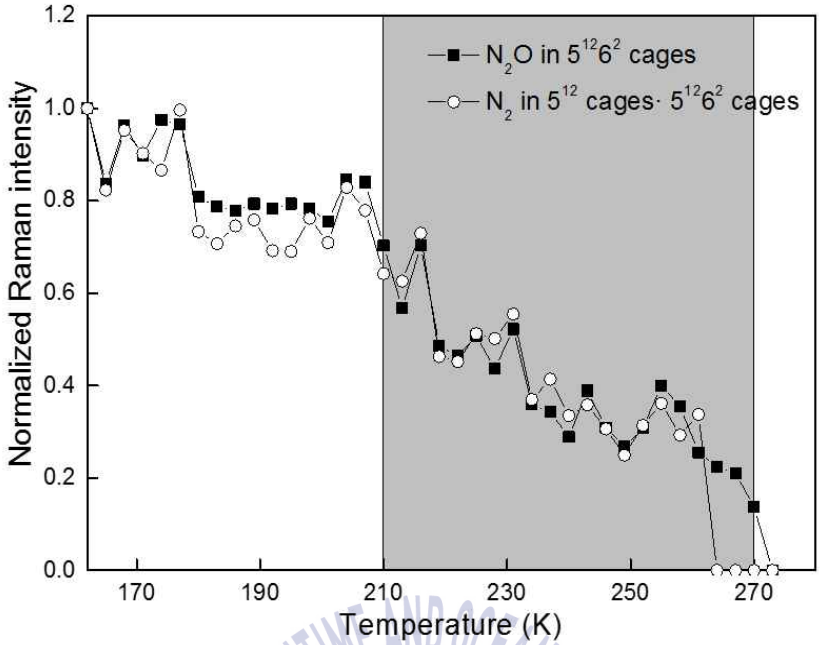

Figure. 17d Normalized relative intensity of Raman peaks for N_2O molecules trapped in large cages and N_2 molecules trapped in small and large cages of N_2O/N_2 (40/60) binary gas hydrate.

I also investigated the dissociation behaviors of N_2O and N_2 guest molecules for another sample, N_2O/N_2 (40/60) binary sI hydrate, in the range of 162-273 K with 3 K intervals using the temperature-dependent Raman spectra. In Figure 17c, Raman band of N_2O molecules at 2218 cm^{-1} in the ν_3 spectral region from the small 5^{12} cages of sI hydrate and Raman band of N−N stretching vibration in N_2 molecules at 2324 cm^{-1} from the large $5^{12}6^2$ cages of sI hydrate were recorded in the temperature range of 162-273 K at ambient pressure condition, and then normalized by the O−H vibration of water molecules (collected at 162 K) at around 3150 cm^{-1}. From 170 to 210 K, there was no significant hydrate dissociation, but N_2O/N_2 (40/60) binary sI hydrate started to rapidly dissociate from 210 K. However, N_2O and N_2 molecules remained in the sI hydrate cages up to 270 K plotted in Figure 17d. It implied that N_2O and N_2 molecules trapped

in N_2O/N_2 (40/60) binary sI hydrate showed the self-preservation behavior in the range of temperature 210–270 K as N_2O encaged in pure N_2O hydrate (Figure 17a). Takeya and Ripmeester reported that CO_2 and N_2 hydrate showed self-preservation phenomena, and thus; self-preservation of pure N_2O sI hydrate and N_2O/N_2 (40/60) binary sI hydrate could be reasonable (Takeya & Ripmeester, 2008).

3.7 Gas Selectivity

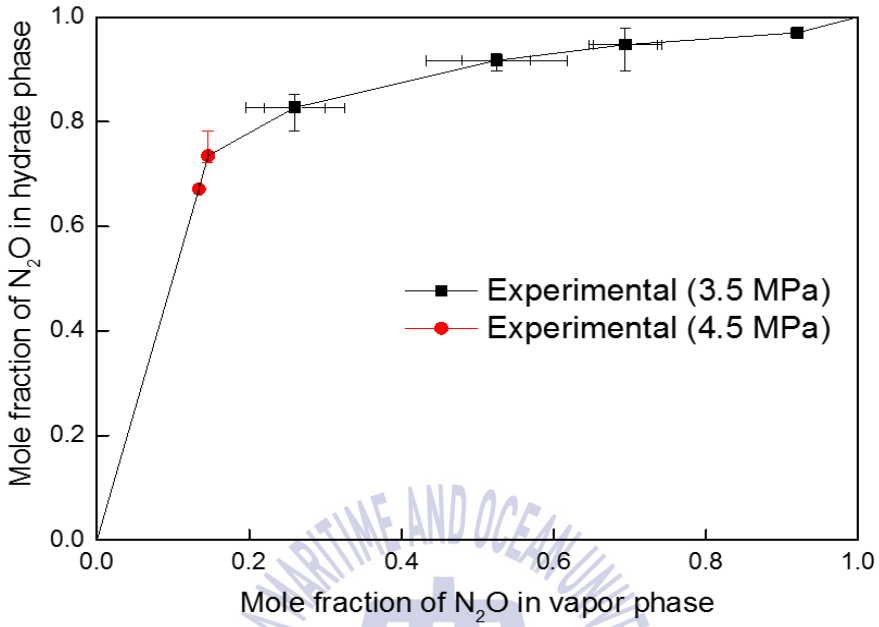

Figure. 18 Fractional concentration of N_2O in N_2O-N_2 binary gas hydrates formed at two-phase (H-V) equilibrium conditions and 268 K.

Even though the high-pressure reactors containing N_2O/N_2 (initial vapor composition: 80/20, 60/40, 40/60, 20/80) gas hydrates were re-charged to desired pressure conditions during hydrate formation, the final vapor composition was changed into 70/30, 55/45, 25/75, and 15/85, respectively, due to the preferential occupation of N_2O in hydrate phases. In other words, the occupation of N_2O in hydrate cages was dominantly occurring in the large cages of sI hydrate. As a result, I successfully demonstrated the amount of N_2O molecules in hydrate phase, as shown in Figure 18.

3.8 Gas Storage Capacity

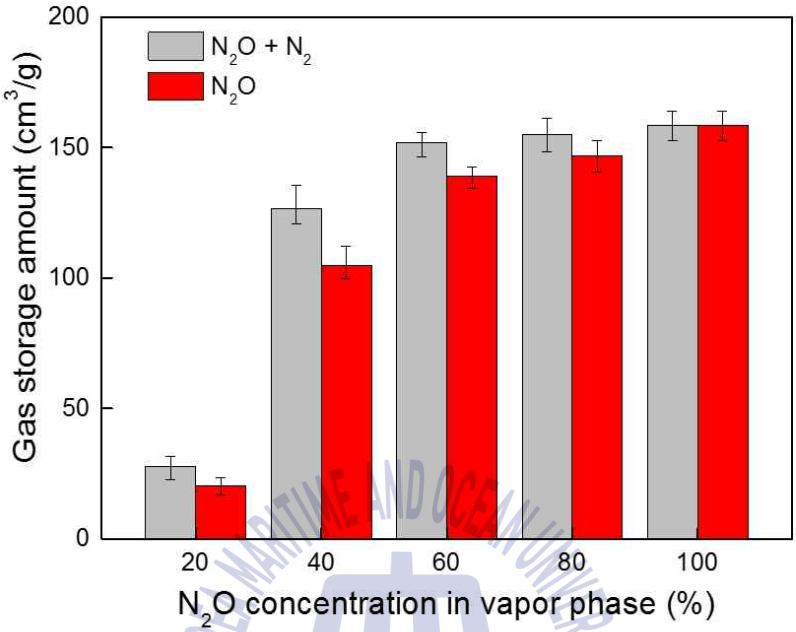

Figure. 19 Gas storage capacity of N_2O-encaged gas hydrates at 268 K. Pure N_2O hydrate was formed at 2.5 MPa and N_2O-N_2 binary gas hydrates were formed at 3.5 MPa (N_2O/N_2 = 80/20, 60/40, 40/60) and 4.5 MPa (N_2O/N_2 = 20/80).

Gas storage capacity of N_2O-N_2 binary gas hydrates under the equilibrium conditions at 268 K and 2.5 MPa for pure N_2O, 3.5 MPa for N_2O/N_2 (80/20, 60/40, 40/60, 20/80) was plotted in Figure 19. For pure N_2O hydrate, the gas storage capacity per a gram of pure N_2O hydrate, approximately 159 cm3/g, were monitored. As the concentration of N_2O in the vapor phase decreased from 100 to 60 mol%, the gas storage capacity of N_2O-N_2 binary gas hydrates was considered to be slightly reduced from 159 to 152 cm^3/g. At the concentration of N_2O 40 % in vapor phase, the gas storage amount rapidly started to decreased, and the amount of gas storage capacity for N_2O/N_2 (20/80) binary gas hydrate was approximately

25 cm^3/g. However, N_2O was still the dominant phase in the hydrate cages as can be seen in diagram of Figure 19.

Chapter 4. Conclusion

In summary, I investigated the structural identification and selective encaging of N_2O in binary gas hydrates formed from N_2O and N_2 mixture gases. The spectroscopic analysis by XRD and Raman spectroscopy confirmed the formation of sI hydrate from N_2O/N_2 (100/0, 80/20, 60/40, 40/60, 20/80) gas mixtures and the preferential occupation of N_2O in hydrate phase. I also observed the inclusion of N_2O in both large and small cages of N_2O/N_2 (100/0, 80/20, 60/40, 40/60) binary sI hydrate whereas N_2O from N_2O/N_2 (20/80) binary sI hydrate occupied only the large cages. From temperature-dependent Raman spectra, I observed the self-preservation of pure N_2O and N_2O/N_2 (40/60) binary gas hydrate in the temperature range of 223-270 K and 210-270 K, respectively, beyond the stability boundary. I identified the phase equilibrium conditions of binary N_2O/N_2 binary gas hydrates. As increasing the concentration of N_2 from 0 to 80 mol% in vapor phase, the three-phase equilibrium (H-Lw-V) of N_2O/N_2 binary gas hydrate were shifted into higher pressure and lower temperature conditions. As the concentration of N_2O in the vapor phase decreases, gas selectivity, gas storage capacity and cage occupancy (θ_L/θ_S) had a similar tendency owing to the preferential occupation of N_2O in the hydrate phase.

This study determines the chemico-physical characteristics of gas hydrates that trap nitrous oxide (N_2O), a greenhouse gas. It presents the sophisticated analysis such as crystal structure, cage occupancy, gas selectivity and phase equilibrium of N_2O-N_2 binary gas hydrates using X-ray diffraction, Raman spectroscopy, Gas chromatography, phase equilibrium measurements, and thermodynamic models. These results and interpretations can be the methodological foundation of selective separation of N_2O from N_2O and N_2 gas mixtures.

Reference

Anderson, A. & Sun, T. S., 1971. Raman spectra of molecular crystals. Carbon dioxide and nitrous oxide. *Chem. Phys. Lett.,* 8, pp.537-542.

Cahill, J. E. & Lerol, G. E., 1969. Raman Spectra of Solid CO_2, N_2O, N_2, and CO. *J. Chem. Phys.,* 51, pp.1324-1332.

Gudmundsson, J. S. Parlaktuna, M. & Khokhar, A. A., 1994. Storing Natural Gas as Frozen Hydrate. *SPE Prod. Facilities*, 9, pp.69-73.

IPCC, 2007. *Climate Change 2007 : Working Group I : The Physical Science Basis* [Available at : https://www.ipcc.ch/publications_and_data/ar4/wg1/en/ch2s2-10-2.html]

Kang, S. P. & Lee, H., 2000. Recovery of CO_2 from Flue Gas using Gas Hydrate: Thermodynamic Verification through Phase Equilibrium Measurements. *Environ. Sci. Technol.,* 34, pp.4397-4400.

Lee, H.-H. et al., 2012. Thermodynamic Stability, Spectroscopic Identification, and Gas Storage Capacity of CO_2-CH_4-N_2 Mixture Gas Hydrates: Implications for Landfill Gas Hydrates. *Environ. Sci. Technol.*, 46, pp.4184-4190.

Lee, Y.-J. Kawamura, T. Yamamoto, Y. & Yoon, J.-H., 2012. Phase Equilibrium Studies of Tetrahydrofuran(THF)+CH_4, THF+CO_2, CH_4+CO_2, and THF+CO_2+CH_4 hydrates. *J. Chem. Eng. Data*, 57, pp.3543-3548.

Linga, P. Kumar, R. & Englezos, P., 2007a. Gas Hydrate Formation from Hydrogen/carbon Dioxide and Nitrogen/carbon Dioxide Gas Mixtures. *Chem. Eng. Sci.,* 62, pp.4268-4276.

Linga, P. Kumar, R. & Englezos, P., 2007b. The Clathrate Hydrate Process for Post and Pre-combustion Capture of Carbon Dioxide. *J. Hazard Mater.*, 149, pp.625-629.

Makogon, Y. F. Holditch, S. A. & Makogon, T. Y., 2007. Natural gas-hydrates-A potential energy source for the 21st Century. *J. Petrol. Sci. Eng*., 56, pp.14-31.

Metz, B. et al., 2007. *Climate Change 2007: Mitigation of Climate Change.* Cambridge University Press: Cambridge, United Kingdom and New York.

Mohammadi, A. H. & Richon, D., 2009. Equilibrium Data of Nitrous Oxide and Carbon Dioxide Clathrate Hydrates. *J. Chem. Eng. Data,* 54, pp.279-281.

Olijnyk, H. Daufer, H. Rubly, M. & Jodl, H.-J., 1990. Effect of pressure and temperature on the Raman spectra of solid N_2O. *J. Chem. Phys.*, 94, pp.45-54.

Pérez-Ramırez, J. et al., 2003. Formation and control of N_2O in nitric acid production: where do we stand today? *Applied Catalysis B: Environmental* 44.2, pp.117-151.

Portmann, R. W. Daniel, J. S. & Ravishankara, A. R. 2012. Stratospheric Ozone Depletion due to Nitrous Oxide: Influences of Other Gases. *Philos. Trans. R. Soc. Lond., B, Biol. Sci.* 367, pp.1256–1264.

Ravishankara, A. R. Daniel, J. S. & Portmann, R. W. 2009. Nitrous Oxide (N_2O): The Dominant Ozone-Depleting Substance Emitted in the 21st Century. *Science* 326, pp.123-125.

Ripmeester, J. A. Tse, J. S. Ratcliffe, C. I. & Powell, B. M. A., 1987. New Clathrate Hydrate Structure. *Nature*, 325, pp.135－136.

Sasaki, S. Hori, S. Kume, T. & Shimizu, H., 2003. Microscopic Observation and In Situ Raman Scattering Studies on High-Pressure Phase Transformations of a Synthetic Nitrogen Hydrate. *J. Chem. Phys.*, 118, pp.7892－7897.

Shin, H. J. et al., 2009. Thermodynamic stability, spectroscopic identification and cage occupation of binary CO_2 clathrate hydrates. *Chem. Eng. Sci.*, 64, pp.5125-5130.

Sloan, E. D., 1988. *Clathrate Hydrates of Natural Gases*, 2nd ed; revised and expanded. Marcel Dekker: New York.

Sloan, E. D., 1998. Gas hydrates: Review of Physical/Chemical Properties. *Energy Fuels*, 12, pp.191-196.

Sloan, E. D., 2003. Fundamental Principles and Applications of Natural Gas Hydrates. *Nature*, 426, pp.353-363.

Sugahara, T. et al., 2009. High-Pressure Phase Equilibrium and Raman Spectroscopic Studies on the Nitrous Oxide Hydrate System. *J. Chem. Eng. Data,* 54, pp.2301-2303.

Sun, Z. et al., 2003, Natural Gas Storage in Hydrate with the Presence of Promoters. *Energy Convers. Manage.,* 44, pp.2733-2742.

Takeya, S. & Ripmeester, J. A., 2008. Dissociation Behavior of Clathrate Hydrates to Ice and Dependence on Guest Molecules. *Angew. Chem. Int. Ed.,* 47, pp.1276-1279.

Udachin, K. A. Ratcliffe, C. I. & Ripmeester, J. A., 2002. Single Crystal Diffraction Studies of Structure I, II and H Hydrates: Structure, Cage Occupancy and Composition. *J. Supramol. Chem.*, 2, pp.405-408.

U.S. Energy Information Administration, 2009. *Emissions of Greenhouse Gases in the United States*, [Available at : http://www.eia.gov/environment/emissions/ghg_report/pdf/0573(2009).pdf

U. S. EPA, 2010. *Methane and nitrous Oxide Emissions from Natural Sources*, [Available at : http://scholars.unh.edu/cgi/viewcontent.cgi?article=1483&context=earthsci_facpub]

van der Walls J. H. & Platteeuw, J. C., 1959. Clathrate Solutions. *Adv. Chem. Phys.*, 2, pp.1-57.

Villard, M., 1888. Sur Quelques Nouveaux Hydrates de Gaz. *Compt. Rend.,* 106, pp.1602-1603.

Villard, M. P., 1897. Etude Experimentale des Hydrates de Gaz. *Ann. Chim. Phys.,* 11, pp.289-394.

von Tammann, G. & Krige, G. J. R., 1925. Die Gleichgewichtsdrucke von Gashydraten. *Z. Anorg. Allg. Chem.,* 146, pp.179-195.

Xu, C.-G. & Li, X.-S., 2014. Research Progress of Hydrate-based CO_2 Separation and Capture from Gas Mixtures. *RSC Adv.*, 4, pp.18301-18316.

Yang, Y, J. et al., 2016. Structural Identification and Cage Occupancy of N_2O-encaged Structure I and II Clathrate Hydrates. *Energy Fuels,* 30, pp.9628-9634.